Increasing Transient Stability Limit by Nonlinear Damping Design

Jinpeng Guo, Haihao Jiang, Xiaozhe Wang, Boon-teck Ooi
Department of Electrical and Computer Engineering
McGill University
Montreal, Canada

SUMMARY

Transient stability sets the limit of power transmissibility. Both the Pacific Intertie and the authors' recent research show that damping power injected by a high voltage direct current (HVDC) station raises the transient-stability limit. Further advance is blocked because the power system is nonlinear from the sin(delta) term in the dynamic equations. In the face of nonlinearity, the graphical phase-plane method is used to shed understanding so that damping power injection can be applied with confidence. The phase-plane method is easy to apply because phase-portraits are obtainable from MATLAB, MATHEMATICA, Wolfram MathWorld and other software providers. Because the phase-plane method is not well known, the method is presented in tutorial fashion. As example, the incidence of a fault and its clearance by circuit breakers are explained by phase-plane portraits representing the pre-fault condition, the fault condition and the post fault condition. The example illustrates how phase-plane portraits can be applied to increase the transient stability limit.

KEYWORDS

Transient Stability Limit, Nonlinear, HVDC Station, Phase Plane, Power Transmissibility

jinpeng.guo@mail.mcgill.ca

I. INTRODUCTION

A. *Transient Stability Limit*

The power transfer capability of a transmission line has constraints which in descending order of magnitude are: the thermal limit, the steady-state limit, the transient-stability limit and system damping [1]. Increasing the transient stability limit brings power transmissibility closer to the thermal limit. For instance, power transmissibility was increased by 20% in the Pacific AC Intertie [2] by injecting damping power from a HVDC station.

B. *Transient Stability Test Platform*

Fig. 1 shows the single-line diagram of the radial power system, which is planned for transient stability test simulations. The turbine-generator delivers power to the infinite bus through transmission Lines 1 and 2. The generator is driven by a speed-regulated turbine. The HVDC station is labeled MMC-HVDC. However, it can be a HVDC station of any generation: thyristor LCC, PWM HVDC as in [2] or the Modular Multilevel Converter (MMC) in [3].

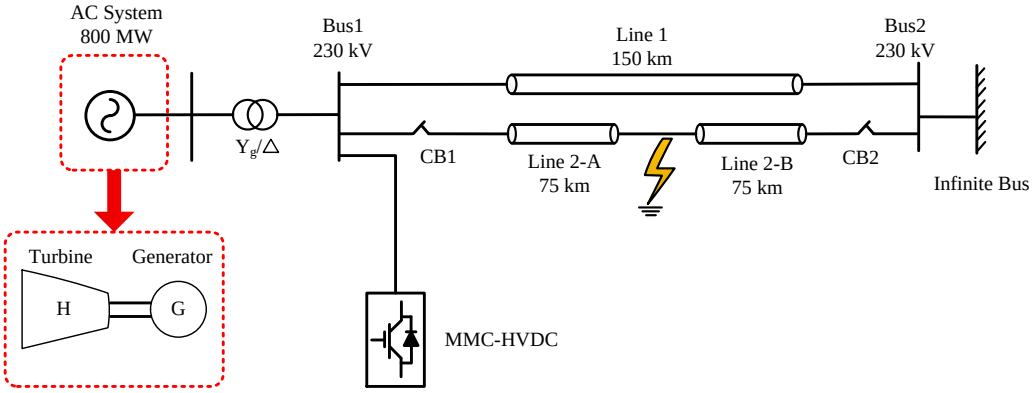

Fig. 1. Transient Stability Test system consisting of MMC-HVDC station connected in shunt to radial transmission line

C. *Transient Stability Test Results*

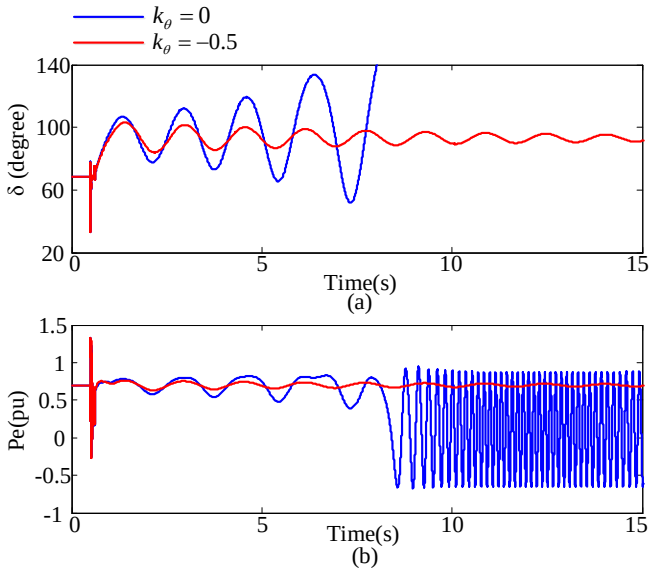

Fig. 2. Transient stability test for P_e=0.7 p.u., k_θ=0 unstable (blue), k_θ =-0.5 stable (red)

In the test, the power from the generator is gradually increased. Initially, the system is stable for feedback gain $k_\theta = 0$ for no damping power injection (blue curve) and for non-zero values of k_θ for damping power injection (red curve). As illustrated in Fig. 2, when the transmitted power is increased to $P_e = 0.7$ p.u., the system is unstable without damping (blue) but is stabilized (red) when the damping gain is $k_\theta = -0.5$.

II. Dynamic Equations of Motion

The transmission system of Fig. 1 is modelled by dynamic equations, taken from page 131 of reference [4]. Using $T_{base} = VA_{base} / \omega_{0m}$, the per unit equations are

$$\frac{2H}{\omega_0}\frac{d^2\delta}{dt^2} = T_m - T_e - \frac{K_D}{\omega_0}\frac{d\delta}{dt} \tag{1}$$

where ω_0 is the frequency of the grid, K_D is the damping coefficient in pu torque/pu speed deviation, T_m is the turbine torque, T_e is the generator counter-torque and where the inertia constant $H = \frac{1}{2}\frac{J\omega_0^2}{VA_{base}}$.

The time derivative

$$\frac{d\delta}{dt} = \omega_r - \omega_0 = \Delta\omega_r \tag{2}$$

On differentiating (2) with respect to time t and combining it with (1) one has the dynamic equation

$$\frac{2H}{\omega_0}\frac{d^2\delta}{dt^2} = T_m - \frac{V^2}{X}\sin\delta - \frac{K_D}{\omega_0}\frac{d\delta}{dt} \tag{3}$$

Equation (3) is simplified as

$$\frac{d\Delta\omega_r}{dt} = A - B\sin\delta - C\Delta\omega_r \tag{4}$$

where $A = \frac{T_m\omega_0}{2H}$, $B = \frac{V^2\omega_0}{2HX}$ and $C = \frac{K_D}{2H}$.

III. Phase-Plane Analysis

A. Phase-Plane Formulation

As there is no analytic solution because of the $\sin\delta$ term in (4), the solution is presented graphically. In (2) and (4), there are two state variables δ and $\Delta\omega_r = d\delta / dt$. Dividing (4) by (2) yields

$$\frac{(\frac{d\Delta\omega_r}{dt})}{(\frac{d\delta}{dt})} = \frac{d\Delta\omega_r}{d\delta} \tag{5}$$

The dimension of time t is removed. Instead, the right-hand side of (5) is a gradient of $\Delta\omega_r$ with respect to δ which on substituting (4) yields

$$\frac{d\Delta\omega_r}{d\delta} = \frac{A - B\sin\delta - C\Delta\omega_r}{\Delta\omega_r} \tag{6}$$

In the 2-D graph of the phase plane portraits, $\Delta\omega_r$ and δ are plotted along the y-axis and the x-axis respectively.

At any point $(\delta, \Delta\omega_r)$ on the graph, $d\Delta\omega_r / d\delta$ is the gradient on of how differential changes in $d\delta$ affect differential changes in $d\Delta\omega_r$. Many software providers such as MATLAB, MATHEMATICA, Wolfram MathWorld etc. provide Phase Plane Plotters. In the paper, the gradients at sampled points $(\delta, \Delta\omega_r)$ on the plane are plotted by the *pplane* program of MATLAB. A gradient has no direction. The arrows are attached based on the following consideration: For $\Delta\omega_r > 0$ above the x-axis, δ must be increasing with time as required by (2). Therefore, the arrows point to the right in the graph above the x-axis. For $\Delta\omega_r < 0$, δ must be decreasing with time and the arrows point to the left. The arrows point to direction only. There is no significance in their lengths [5], [6].

B. Phase-Plane Portraits

The phase-plane portraits are presented in Fig. 3 to Fig. 6 for operating conditions characterized by coefficients *A*, *B* and *C* of (4), which are shown in Table I. In the following, *A* and *B* are normalized based on $V^2\omega_0 / (2HX)$.

TABLE I. PARAMETERS OF THE PHASE-PLANE PORTRAITS

Figures	*A*	*B*	*C*	Remarks
3	0	1.0	0	Limit cycles and unstable regions outside separatices.
4	0	1.0	0.5	Damping brings system to focuses as operating points
5	0.4	1.0	0.5	Effect of *A* to shift δ
6	0.4	0.1	0.5	Destabilization during transmission line fault

Example: *A*=0, *B*=1.0 and *C*=0

The phase plane portrait for the system with parameters *A*=0 (no turbine torque), *B*=1.0 and *C*=0 (no damping torque) is shown in Fig. 3.

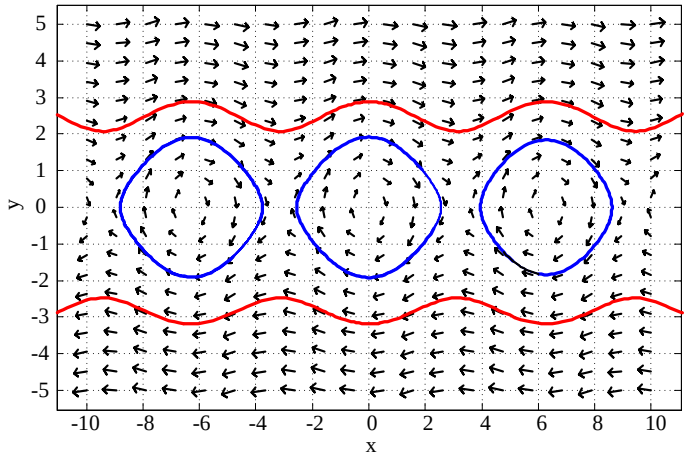

Fig. 3. Phase-plane portrait of $d\Delta\omega_r / d\delta$ when *A*=0, *B*=1.0 and *C*=0

In Fig. 3, the trajectories are elliptical limit cycles with centres around $\delta = -2\pi$, δ=0 and $\delta = 2\pi$. Because $\sin\delta = \sin(\delta + 2n\pi)$, the limit cycles are bounded in 3 regions: $(-\pi \le \delta + 2\pi \le \pi)$, $(-\pi \le \delta \le \pi)$ and $(-\pi \le \delta - 2\pi \le \pi)$. Because the denominator of

(6) is $\Delta\omega_r$, for high values of $|\Delta\omega_r|$ the gradients are small. The regions of high $|\Delta\omega_r|$ are separated from the limit cycles by separatrices (red lines). The regions outside the separatrices are unstable because the trajectories do not converge to the limit cycles or focuses. The system becomes unstable when a disturbance causes $\Delta\omega_r$ to lie outside the separatrice.

Example: A=0, B=1.0 and $C = 0.5$

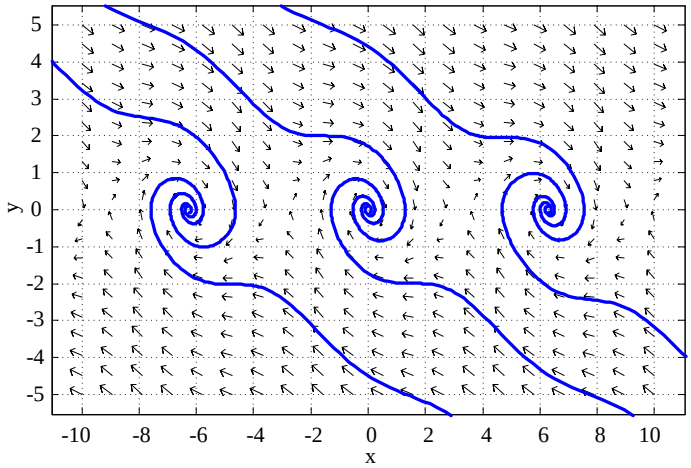

Fig. 4. Phase-plane portrait of $d\Delta\omega_r / d\delta$ when A=0, B=1.0 and C=0.5

Positive damping of parameter C=0.5 is introduced and the results are shown in Fig. 4. The C term of (6) shifts the gradients of Fig. 3 to the right in the direction of the arrows. The shift angle increases with the magnitude of C. The trajectories are no longer limit cycles but converge as spirals to the equilibrium points [$\delta_0 = 0 + 2\,\mathrm{n}\,\pi$, $\Delta\omega_r = 0$] $n = -1, 0, +1$. Regions in the unstable region of Fig. 3, which lie outside separatrices, can converge to the equilibrium points. Trajectories can cross regions: $(-\pi \le \delta + 2\pi \le \pi)$, $(-\pi \le \delta \le \pi)$ and $(-\pi \le \delta - 2\pi \le \pi)$. Physically, crossing from one region to the next means gaining or slipping rotation of one pole-pair of the generator.

Example: A=0.4, B=1.0 and C=0.5

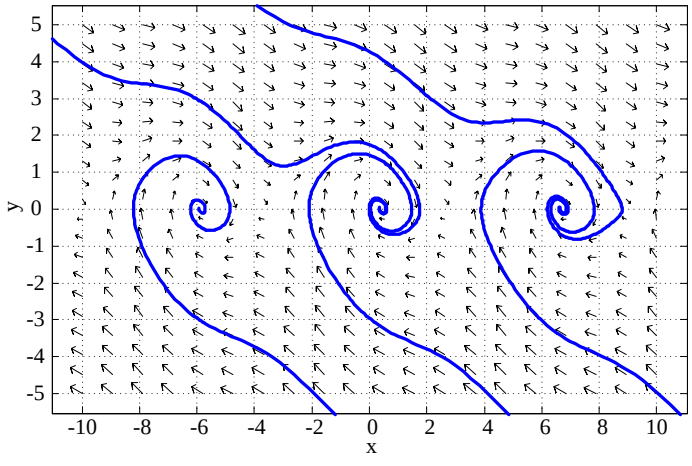

Fig. 5. Phase-plane portrait of $d\Delta\omega_r / d\delta$ when A=0.4, B=1.0 and C=0.5

$A \neq 0$ means that turbine torque T_m of (1) is considered in the phase-plane portrait. The effect of turbine torque is illustrated by setting parameter A=0.4. From (4), the equilibrium lies on $\delta = arc\sin(A/B)$. Fig. 5 shows the portrait for the case of A=0.4, B=1.0 and C=0.5.

The turbine torque shifts the equilibrium torque angle from $\delta = 0$ in Fig. 3 and 4 to $\delta = 0.41$ or 23°.

Example: A=0.4, B=0.1 and C=0.5

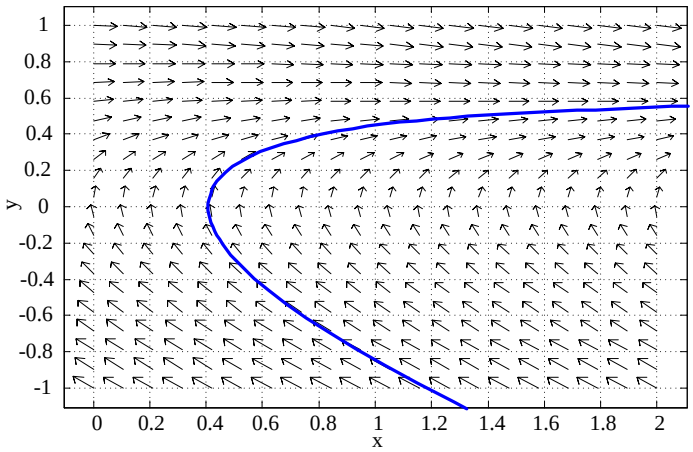

Fig. 6. Phase-plane portrait of $d\Delta\omega_r / d\delta$ when A=0.4, B=0.1 and C=0.5

As for the system described by Fig. 5, if the voltage drops during a short circuit fault, $B = V^2\omega_0 / 2HX$ is lowered from B=1.0 to B=0.1, for example. Fig. 6 corresponds to the period between the occurrence of the fault and its clearance by circuit breakers. This period is unstable because the direction of the arrows shows that there is no convergence. In the fault period of Fig. 6, the trajectory leaves [$\delta(t_1) = 0.41$, $\Delta\omega_r(t_1) = 0$] at time t_1. Modern fast circuit breakers enable the trajectory to terminate at time t_2 at state-variables [$\delta(t_2)$, $\Delta\omega_r(t_2)$] within 5 cycles of the supply frequency.

Phase portraits give static overviews. The transition from initial states [$\delta(t_1) = 0.41$, $\Delta\omega_r(t_1) = 0$] to the terminal states [$\delta(t_2)$, $\Delta\omega_r(t_2)$] requires simultaneous numerical integration of (2) and (4) to arrive at t_2=t_1+100 ms for the 5 cycles of 50 Hz between the incidence of the fault and its clearance by circuit breakers. Once the fault is cleared, the power is transmitted only along Line 1. The parameter B is changed and detailed analyses are given in section IV.

IV. Integration Phase-Plane Portraits in Transient Stability Test

A. Prior to Fault

Prior to the transmission line fault, the system has been at rest at state-variables [$\delta(t_1) = 0.41, \Delta\omega_r(t_1) = 0$] at time t_1 in Fig. 5.

B. Transmission Line Fault

In a 3-phase short-circuit ground fault in Fig. 1, the voltage drops so that B is lowered to $B = V^2\omega_0 / 2HX = 0.1$, for example. In Fig. 6, the parameters are A=0.4, B=0.1 and C=0.5. The system leaves [$\delta(t_1) = 0.41, \Delta\omega_r(t_1) = 0$] at time t_1 along the trajectory in the y > 0 region. This trajectory is unstable. Because of the development of fast circuit breakers, the fault is cleared within five 50 Hz cycles. The final state is [$\delta(t_2), \Delta\omega_r(t_2)$] at time t_2. In the five 50 Hz cycles, the final state [$\delta(t_2)$, $\Delta\omega_r(t_2)$] is close to the initial state [$\delta(t_1) = 0.41, \Delta\omega_r(t_1) = 0$].

The simultaneous numerical integration of (2) and (4) yields $[\,\delta(t_2)=0.412\,,\Delta\omega_{\mathrm{r}}(t_2)=0.035\,]$ as the final state.

C. Post Fault

On clearing the fault, the voltage returns to the rated value but power is transmitted along Line 1 only in Fig. 1. However, the reactance increases since there is only one transmission line, as shown in Fig. 1. The parameters of the phase-plane are changed to *A*=0.4, *B*=0.5 and *C*=0.5 for example. Fig. 7 is the phase portrait.

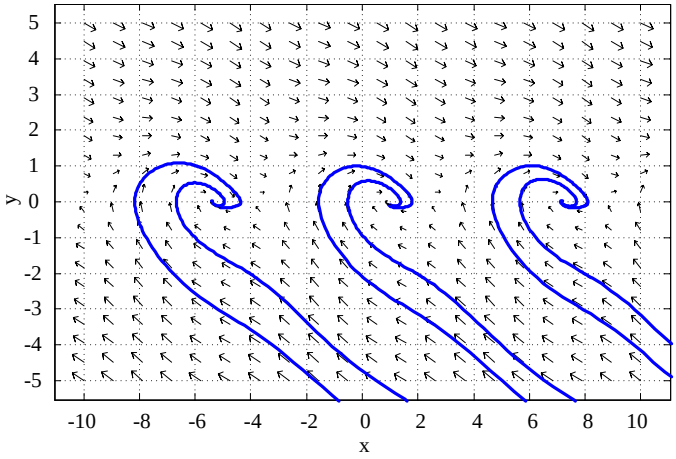

Fig. 7. Phase-plane portrait of $d\Delta\omega_{\mathrm{r}}/d\delta$ when *A*=0.4, *B*=0.5 and *C*=0.5

The trajectory of Fig. 6 brings the system to higher rotor speed, which is measured as $\Delta\omega_{\mathrm{r}}(t_2)$. The initial states of the post fault system are taken from the final state-variables $[\,\delta(t_2)=0.412\,,\Delta\omega_{\mathrm{r}}(t_2)=0.035\,]$ of Fig. 6. In the example, as $\Delta\omega_{\mathrm{r}}(t_2)=0.035<1.0$ in Fig. 7, there is convergence to steady-state equilibrium. Physically it means that since $\Delta\omega_{\mathrm{r}}(t_2)=0.035$ is close to $\Delta\omega_{\mathrm{r}}=0$, damping power dissipates the excess kinetic energy and lowers the rotor speed to $\Delta\omega_{\mathrm{r}}(t_3)=0.0$.

Fig. 5, 6 and 7 are archetype phase-plane portraits for designing nonlinear damping to extend the transient stability limit. Design begins with the value of *C* which the HVDC station or FACTS controller can achieve. The objective is to maximize *A* while respecting *B* which changes with operating conditions.

V. CONCLUSIONS

Nonlinearity is a barrier to understanding how the transient stability limit and hence power transmissibility can be increased by injecting damping power. The phase plane method, which can give a graphical insight into the nature of the nonlinear problem, is applied to to disclose the role of nonlinear damping in increasing transient stability limit.

Phase-plane portrait shows that without damping, the turbine-generator system executes bounded limit cycles. If a disturbance causes rotor speed, $\Delta\omega_{\mathrm{r}}$, to lie outside the separatrice bounds, the system becomes unstable. Damping shifts trajectories to the right in the direction of the phase-plane, so that instead of executing limit cycles, the system is damped to converge to a steady-state operating point.

Phase-plane portraits present a comprehensive view that

(a) when a disturbance causes rotor speed, $\Delta\omega_{\mathrm{r}}$, to increase, damping power reduces the

perturbation speed until the equilibrium $\Delta\omega_r = 0$ is reached.

(b) equilibrium at $\delta = \arcsin(A/B)$ is always reached, in many cases by exceeding the $(-\pi \le \delta \le \pi)$. This involves gaining or slipping one or more pole-pair of the generator.

Since phase-plane portraits are available from software providers (MATLAB, MATHEMATICA, Wolfram MathWorld, etc.) and are computed quickly, they are tools for iterative design of

(a) the extent by which the turbine power *A* can be increased.
(b) for the damping power *C* which is available.

BIBLIOGRAPHY

[1] R. Mohan Mathur and Rajiv K. Varma, Thyristor-Based FACTS Controllers for Electrical Transmission Systems. New York, USA: Wiley Science, 2002.

[2] R. L. Cresap, W. A. Mittelstadt, D. N. Scott and C. W. Taylor, "Operating Experience with Modulation of the Pacific HVDC Intertie," in IEEE Transactions on Power Apparatus and Systems, vol. PAS-97, no. 4, pp. 1053-1059, July 1978.

[3] F. Badrkhani Ajaei and R. Iravani, "Dynamic Interactions of the MMC-HVDC Grid and its Host AC System Due to AC-Side Disturbances," in IEEE Transactions on Power Delivery, vol. 31, no. 3, pp. 1289-1298, June 2016.

[4] P. Kundur, Power System Stability and Control. New York, USA: McGraw-Hill, 1994.

[5] G.J. Thaler and R.G. Brown, Analysis and Design of Feedback Control Systems. New York, USA: McGraw-Hill, 1962.

[6] D.W.Jordan, P.Smith, Nonlinear Ordinary Differential Equations: Introduction to Scientists and Engineers. Oxford, UK: Oxford University Press, 2007.